

Structural Rearrangements of the Central Region of the Morbillivirus Attachment Protein Stalk Domain Trigger F Protein Refolding for Membrane Fusion^{*[5]}

Received for publication, January 13, 2012, and in revised form, March 17, 2012. Published, JBC Papers in Press, March 19, 2012, DOI 10.1074/jbc.M112.342493

Nadine Ader[‡], Melinda A. Brindley[§], Mislav Avila[‡], Francesco C. Origgi[¶], Johannes P. M. Langedijk^{||}, Claes Örvell^{**}, Marc Vandeveld^{**}, Andreas Zurbriggen[‡], Richard K. Plemper^{§§}, and Philippe Plattet^{‡1}

From the [‡]Division of Experimental Clinical Research, Neurovirology Unit, DCR-VPH, Vetsuisse faculty, University of Bern, 3001 Bern, Switzerland, the [§]Department of Pediatrics, Emory University School of Medicine, Atlanta, Georgia 30322, the ^{§§}Children's Healthcare of Atlanta, Atlanta, Georgia, the ^{¶¶}Division of Neurology, DCV, Vetsuisse Faculty, University of Bern, 3001 Bern, Switzerland, the ^{¶¶}Centre for Fish and Wildlife Health (FIWI)-ITPA, DIP, Vetsuisse Faculty, University of Bern, 3012 Bern, Switzerland, ^{||}Innovation and Discovery Laboratory, Crucell Holland B.V., Archimedesweg 4-6, PO Box 2048 2301 CA, Leiden, and the ^{**}Laboratory of Clinical Virology, Karolinska University Hospital Huddinge, SE-19186 Stockholm, Sweden

Background: Attachment (H) and fusion glycoproteins of morbilliviruses co-operate to induce membrane fusion for cell entry.

Results: Reversible membrane fusion inhibition by engineered disulfide bonds within the central region of the tetrameric H-stalk domain.

Conclusion: Structural rearrangements of the H-stalk domain contribute to fusion triggering.

Significance: Provides a basis for novel strategies targeting the central region of the attachment protein-stalk domain to prevent Morbillivirus cell entry.

It is unknown how receptor binding by the paramyxovirus attachment proteins (HN, H, or G) triggers the fusion (F) protein to fuse with the plasma membrane for cell entry. H-proteins of the morbillivirus genus consist of a stalk ectodomain supporting a cuboidal head; physiological oligomers consist of non-covalent dimer-of-dimers. We report here the successful engineering of intermolecular disulfide bonds within the central region (residues 91–115) of the morbillivirus H-stalk; a sub-domain that also encompasses the putative F-contacting section (residues 111–118). Remarkably, several intersubunit crosslinks abrogated membrane fusion, but bioactivity was restored under reducing conditions. This phenotype extended equally to H proteins derived from virulent and attenuated morbillivirus strains and was independent of the nature of the contacted receptor. Our data reveal that the morbillivirus H-stalk domain is composed of four tightly-packed subunits. Upon receptor binding, these subunits structurally rearrange, possibly inducing conformational changes within the central region of the stalk, which, in turn, promote fusion. Given that the fundamental architecture appears conserved among paramyxovirus attachment protein stalk domains, we predict that these motions may act as a universal paramyxovirus F-triggering mechanism.

The Paramyxoviridae family is composed of enveloped, non-segmented negative-stranded RNA viruses, which include

many important pathogens such as mumps virus, Newcastle disease virus (NDV)², parainfluenza viruses, the recently emerged, highly pathogenic henipaviruses, and the morbilliviruses. A member of the latter genus, Measles virus (MeV) accounts for more than 120,000 fatalities each year (1) and canine distemper virus (CDV) causes diseases with high morbidity and mortality in domestic, wild, and aquatic carnivores. Viruses of the *Paramyxovirinae* subfamily contain two envelope glycoproteins that tightly co-operate for viral cell entry and spread: the attachment and the fusion proteins. The attachment proteins mediate receptor binding and promote membrane fusion by triggering the fusion protein. Whereas HN attachment proteins bind to sialic acid-containing cell surface molecules, H and G contact proteinaceous receptors (2–7). In addition, HN-proteins contain neuraminidase activity (8).

MeV and CDV H-proteins are type II transmembrane glycoproteins, which consist of an N-terminal cytosolic tail, a short single membrane-spanning region and a large ectodomain. The extracellular domain encompasses a membrane-proximal stalk region that supports a terminal cuboidal head contacting the receptors. The head domain of MeV H has been crystallized in the presence and absence of receptors and invariably shows a very similar six-bladed β -propeller fold, with blades 4, 5, and 6 involved in binding to multiple receptors (CD150/SLAM and CD46) (9–12). Moreover, structural and functional studies revealed that the H-protein oligomeric organization consists of tetramers and/or higher order oligomers (13). H-tetramers are composed of a loosely associated dimer of covalently linked dimers (9, 13, 14). Two naturally occurring intersubunit disul-

^{*} This work was supported by the Swiss National Science Foundation (Ref. No. 310030_132887; to P. P.) and, in part, by United States Public Health Service Grant AI083402 (to R. K. P.).

^[5] This article contains supplemental Figs. S1–S4.

¹ To whom correspondence should be addressed: Bremgartenstrasse 109a, 3001 Bern, Switzerland. Tel.: 4131-631-26-48; Fax: 4131-631-25-38; E-mail: philippe.plattet@vetsuisse.unibe.ch.

² The abbreviations used are: NDV, Newcastle disease virus; MeV, measles virus; CDV, canine distemper virus; 4HB, four helix bundle; MFI, mean fluorescence intensity.

disulfide bonds are located at the top of the stalk domain (Cys-139 and Cys-154) (14).

Recently, x-ray structures of partial regions of the Newcastle disease virus (NDV) and Parainfluenza virus type 5 (PIV5) HN-stalk domains revealed that the stalk folds as a four helix bundle (4HB) with a supercoiled membrane-proximal region that contains a 7-residue repeat (PIV5) and a membrane-distal straight region characterized by an 11-residue repeat (PIV5 and NDV) (15, 16). The stalk domain of the attachment protein of many paramyxoviruses has been reported to contribute to physical interaction with F (17–23). In the case of the MeV H-stalk domain, residues 111–118 are thought to support short-range interaction with MeV F (23). In contrast, the precise reciprocal domain(s) in F that contact(s) the attachment protein remains to be identified, though several investigations suggested domains in the F-head as putative candidates (23–26). Based on recent functional and biochemical evidence, it has been proposed that the morbillivirus tetrameric H-stalk domain might also fold into an extended straight structure, which inferred a staggered H/F spatial organization with the H-heads positioned above the trimeric fusion protein (27).

Central in promoting efficient viral-cell entry are specific interactions between the receptor, attachment, and F glycoproteins which, in concert, control the location and timing of the fusion process (8). According to a current paradigm of paramyxovirus cell entry, the attachment protein undergoes conformational modifications upon receptor binding that trigger refolding of the fusion protein, which is directly coupled to membrane fusion (28, 29). Despite intensive investigations, however, the nature of the rearrangements in the attachment protein that trigger F refolding remains largely unknown. Interestingly, minor adjustments within the MeV H dimeric head interface have been recently proposed as an early F-triggering event (30).

In view of the close interaction between the head of the morbillivirus F-protein and the putative extended tetrameric H-stalk conformation, we hypothesized that receptor binding may induce a structural rearrangement of the stalk leading to the triggering of F. To test this, we targeted the highly conserved central region of the CDV H-stalk domain (91–115), which also encompasses the putative F-contacting domain (111–118) (23, 27), and performed a comprehensive cysteine-scanning mutagenesis. This strategy aimed to restrict mobility of the H-stalk monomers through the introduction of supplementary disulfide bonds either within existing dimers (thus reinforcing the natural bonds) or the dimer-of-dimers (thus generating covalently linked tetramers). Indeed, in the putative “pre-receptor bound” native state of H, some cysteine mutants efficiently generated covalent dimers and tetramers. Several of these engineered crosslinks strongly abrogated membrane fusion, but inhibition could be overcome by partial reduction of disulfide bonds. Moreover, these results were obtained with attachment proteins derived from virulent and attenuated CDV as well as MeV strains, and were independent of the nature of the contacted receptor.

Overall, our results support the view that prior to receptor binding, the morbillivirus H-stalk domain is composed of four compact subunits, consistent with a 4HB conformational state

reminiscent of the NDV and PIV5 HN-stalk structures. Receptor-binding induces significant structural rearrangements in the central region (98–109) of the putative tetrameric morbillivirus H-stalk domain that appear required for the promotion of membrane fusion. A new model is proposed to clarify how these rearrangements may trigger plasma membrane fusion.

EXPERIMENTAL PROCEDURES

Cell Cultures and Viruses—Vero, Vero cells expressing the canine SLAM receptor (Vero-cSLAM), Vero cells expressing the human SLAM receptor (Vero-hSLAM; kindly provided by Y. Yanagi, Kyushu University, Japan) and 293T cells were grown in Dulbecco’s modified Eagle’s medium (Invitrogen) with 10% fetal calf serum at 37 °C in the presence of 5% CO₂. The MVA-T7 recombinant vaccinia virus used for a quantitative cell-cell fusion assay was kindly provided by B. Moss, NIH, Bethesda, MD.

Construction of Expression Plasmids—All single (and multiple) substitutions performed in pCI-HwteF (derived from hemagglutinin of the A75/17 CDV strain (31)) and in pCI-HOPeF (derived from the hemagglutinin of the Onderstepoort CDV strain, (31)) were obtained using the QuikChange lightning site-directed mutagenesis kit (Stratagene). The cDNA of MeV-H edmonston strain and MeV-H WTFb strain (kindly provided by Jürgen Schneider Schaulies, Würzburg, Germany) were subcloned into the pCI vector using conventional molecular methods. The pCI-H301FeF vector was previously described and encodes the hemagglutinin protein derived from a recently fox-isolated CDV strain (W10/301/red-fox/Ch/2010-JF810106 and referred in this study to as 301F) (32). To produce a soluble form of Hwt^{eF}, the complete ectodomain was cloned in-frame with the IgK signal peptide. In addition, to maximize the prospect of preserving the H-tetramer oligomeric state in its soluble form, the dimeric/tetrameric GCN4 peptide (33, 34) was fused N-terminally as well as a 6-histidine tag (6×His). Production of the H soluble form (sol. H) was obtained following transfection of 293T cells with the expression vector. 72 h post-transfection, the supernatant was harvested and concentrated with a 30-kDa cutoff column (Millipore). His-tagged soluble H materials were then purified with the nickel/magnetic beads system (Qiagen). All H proteins were also contained a C-terminal FLAG tag (31, 35). All MeV F and H expression plasmids were kindly provided by Jürgen Schneider-Schaulies (Würzburg, Germany).

Transfections, Dithiothreitol (DTT) Treatment, and Luciferase Reporter Gene Content Mix Assay—Vero cells, in 6-well plates at 90% confluency, were co-transfected with 2 μg of the pCI-F^{wT} constructs and 1 μg of the various pCI-H-expressing plasmids with 9 μl of Eugene HD (Roche). Vero cells in 24 wells or 6 wells were transfected with 1 or 3 μg of the various pCI-H plasmids with 3 or 9 μl of Eugene HD. All transfections were performed according to the manufacturer’s protocol. In some experiments, representative phase contrast pictures were taken 24 h post-transfection with a confocal microscope (Olympus, Fluoroview, FV1000).

To assess whether engineered disulfide bonds might have been formed, Vero-cSLAM cells were transfected as mentioned above. Four hours post-transfection, the medium was replaced

Motion within the Morbillivirus H-stalk Triggers Fusion

by medium containing 50 μM fusion inhibitory molecule (3g) (36, 37). Twenty-four hours post-transfection, cells were washed and incubated 30 min in PBS or PBS containing 15 mM DTT. Subsequently, cells were washed and incubated in normal medium at 37 °C. Fusion activity was assessed 3 h post DTT treatment. Representative phase contrast pictures were taken with a confocal microscope (Olympus, Fluoroview, FV1000).

The quantitative fusion assay was performed as described previously (38, 39) with subtle modifications. Briefly, Vero cells were co-transfected with the F and H expression plasmids and 0.1 μg of pTM-Luc (kindly provided by Laurent Roux, University of Geneva). In parallel, separate 6-well plates of Vero-cSLAM cells at 30% confluency were infected with MVA-T7 (40) at a multiplicity of infection (MOI) of 1. After overnight incubation, both cell populations were mixed and incubated at 37 °C for 2 h in medium containing 50 μM of 3g. Subsequently, cells were washed three times and further incubated for 30 min at 37 °C in PBS containing, or not, 15 mM DTT. Cells were washed three times with PBS and incubated at 37 °C in normal medium. Three hours later, the cells were lysed using Bright Glo Lysis Buffer (Promega), and the luciferase activity was determined using a luminescence counter (PerkinElmer Life Sciences) and the Britelite reporter gene assay system (PerkinElmer Life Sciences).

Western Blotting—Western blots were performed as previously described (39). Twenty-four hours post-transfection, cells were treated for 1 h at 4 °C with anti-FLAG mAb (1/500) (Sigma Aldrich: F3165). Cells were lysed with 150 μl of lysis buffer (10 mM Tris, pH 7.4, 150 mM NaCl, 1% deoxycholate, 1% Triton X-100, 0.1% sodium dodecyl sulfate (SDS)) with complete protease inhibitor (Roche Biochemicals). Cleared lysates were incubated overnight with immunoglobulin G-coupled Sepharose beads (GE Healthcare). The precipitates were subsequently boiled at 95 °C for 5 min and fractionated alternatively on 8 or 10% SDS-polyacrylamide Tris-glycine gels. Separated proteins were transferred to nitrocellulose membranes by electroblotting. The membranes were then incubated either with the polyclonal rabbit anti-HA antibody (16B12, Covance), anti-F antibody, anti-H antibody (41) or monoclonal anti-H 1347 antibody (41). Following incubation with a peroxidase-conjugated secondary antibody, the membranes were subjected to enhanced chemiluminescence (ECL) kit (Amersham Biosciences) according to the manufacturer's instructions.

To efficiently discriminate between the large molecular weight of H-dimers and H-tetramers under denaturing conditions, cell surface proteins (prepared as described above) were fractionated on 3–8% (gradient) Tris-acetate gels under nonreducing conditions (w/o DTT). The samples were then subjected to Western blot analysis as described above.

F/H Co-immunoprecipitation—F/H Co-immunoprecipitations were performed as previously described (35). At 24 h post-transfection, the cells were washed with cold PBS and treated with DTSSP (1 mM final concentration in PBS, Sigma Aldrich). Cells were subsequently lysed in RIPA buffer (10 mM Tris, pH 7.4, 150 mM NaCl, 1% deoxycholate, 1% Triton X-100, 0.1% sodium dodecyl sulfate (SDS)) containing protease inhibitors (Roche, complete mix). Cleared lysates (20,000 \times g; 20 min; 4 °C) were incubated with an anti-CDV-H monoclonal anti-

body 1347 (42), followed by overnight incubation with immunoglobulin G-coupled Sepharose beads (GE Healthcare). The samples were then subjected to Western blot analysis as described above using either the polyclonal anti-H or the anti-F antibody (41).

Cell Surface Expression and SLAM Binding Activity—To determine the cell surface expression of the various H-proteins, Vero cells were first transfected with 1 μg of H-expression plasmids. One day post-transfection, unfixed and unpermeabilized cells were washed twice with ice-cold PBS and subsequently stained with an anti-FLAG mAb (Sigma Aldrich: F3165). This was followed by washes with ice-cold PBS and incubation of the cells with Alexa-fluor 488-conjugated secondary antibody (Invitrogen) (1:500) for 1 h at 4 °C. Cells were washed five times with ice-cold PBS and subsequently detached from the wells by adding PBS-EDTA (50 μM) for 30 min at 37 °C. The mean fluorescence intensity (MFI) of 10,000 cells was then measured by using a BD LSRII flow cytometer (Becton Dickinson).

SLAM binding activity was performed as previously described (31). Briefly, H-protein-expressing cells were incubated for 1 h at 4 °C with soluble HA-tagged canine SLAM molecules, followed by three PBS washes and treatment with anti-HA mAb (1/1000) (Covance: 16B12, 1 h at 4 °C). Cells then were incubated with the Alexa-fluor 488-conjugated secondary antibody and were submitted to flow cytometry as described above. Relative SLAM-binding activity of the different H proteins was determined by dividing MFI values recorded with the anti-HA mAb (SLAM-binding efficiency) by MFI values recorded with anti-FLAG mAb (cell surface expression). An arbitrary value equal to 100% binding activity was assigned to that occurring between Hwt and SLAM.

Homology Modeling—Homology modeling was based on sequence alignment of CDV-HA75/17 and the homologous template of the native four-helix bundle of hPIV5 (15), using the automated protein-modeling software provided by the SWISSMODEL protein-modeling server (43, 44). According to the alignment shown in Fig. 6E, only one residue had to be inserted at position 91 in the superhelical region of the bundle to construct the model. As a result the secondary structure of the helix was interrupted at this position because of the loss of hydrogen bonds at one helical turn. This interruption does not affect the visualization of the mutants because it is just N-terminal to the mutated region of the stalk (Fig. 1D). Because the hPIV5 template is not symmetrical, the helices of the CDV H bundle do not have the same lengths and range from residues 53/56 to residues 103/109.

RESULTS

Cell Surface Expression and Receptor Binding Activity of Morbillivirus H-proteins with Cysteine Substitution within the Central Region of the Stalk Domain—Recent structural insight into the spatial organization of the tetrameric MeV H-head inferred stalk rearrangement for F-triggering upon receptor-binding: a pre-formed tetrameric stalk dissociates into two dimers (Fig. 1A) (9). In this study, we explored whether the native stalk subunits are organized into a compact tetrameric structure that undergoes receptor-induced structural rearrangements resulting in membrane fusion triggering. To test this, we subjected

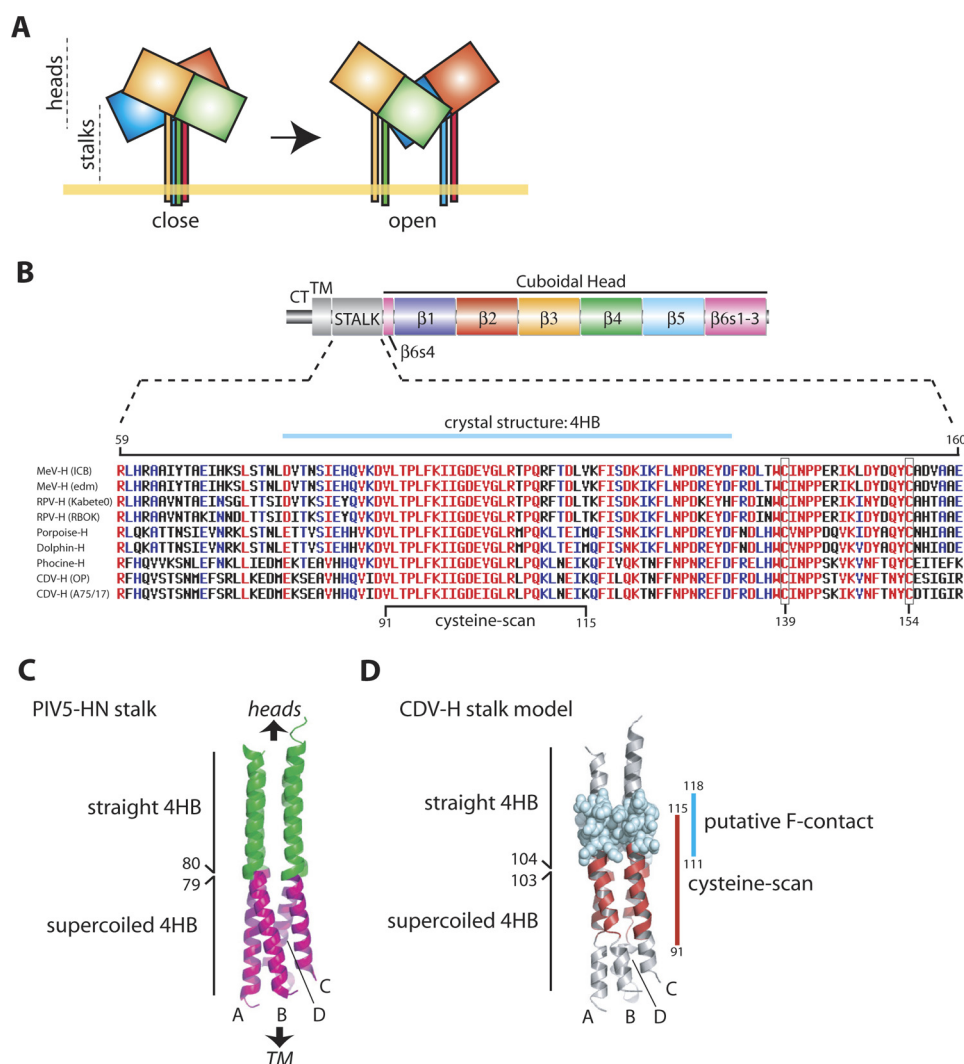


FIGURE 1. The central section of the morbillivirus H-stalk is highly conserved. *A*, model of H-stalk motion upon receptor binding: a pre-formed tetrameric H-stalk (*close*) dissociates after receptor interaction (*open*). Each monomer of the H-tetramer is highlighted with different colors. *B*, *upper panel*: primary structure of the H-protein; CT, cytoplasmic tail; TM, transmembrane region; β 1– β 6, color-coded β -propeller blades 1–6. The four β -strands of blade 6 are indicated. *Lower panel*: sequence alignment of the amino acids of the H-proteins' stalk domain of different morbilliviruses. GenBankTM numbers for each virus sequence are: AB016162.1 (measles, ICB strain), AF266288.1 (measles, Edmonston strain), AF305419.1 (canine distemper, Onderstepoort strain), AY386316.1 (canine distemper, A75/17 strain), X98291.3 (rinderpest virus, Kabete O strain), Y18816.1 (rinderpest virus, K strain), FJ648457.1 (porpoise morbillivirus, IRL88 strain), FJ648456.1 (phocine distemper virus, DK02 strain), NC_005283.1 (dolphin morbillivirus). Red, blue, and black colors represent highly conserved, semi-conserved, and less conserved residues, respectively (15). Cysteines 139 and 154 at the top of the Morbillivirus H-stalk domain involved in natural disulfide bonds are shown (boxes). *C*, side view of the PIV5 HN-stalk structure. The upper 4HB straight structure is shown in green, the lower superhelical region in purple. *D*, structural model of the CDV H-stalk (*side view*). The region subjected to cysteine-scanning mutagenesis is highlighted in red. Putative F-contacting region (111–118) is shown in blue (23).

the central H-stalk segment to a comprehensive cysteine-scanning mutagenesis in the attempt to potentially stabilize the presumptive tetrameric stalk structure through newly formed intermolecular disulfide bonds. The central region (residues 91–115) of the stalk was selected for this approach for three main reasons: (i) the high conservation of the motif 90–109 (Fig. 1*B*), (ii) according to the recently determined PIV5 HN-stalk crystal structure, the central region encompasses a structural boundary between a membrane-proximal superhelical and a membrane-distal straight 4HB conformation (Fig. 1*C*) (15), and (iii) MeV H residues 111–118 of the stalk domain are thought to contribute to physical interaction with F (Fig. 1*D*) (23, 27).

We used the H-protein of the highly neurovirulent A75/17-CDV strain as a morbillivirus attachment protein model. To

gain a structure/function understanding of key residues, we first generated a structural model of the CDV H-stalk domain using the PIV5 HN-stalk atomic structure as a template (Fig. 1*C*). When highlighted in the model, the residues postulated to contribute to F binding map to the membrane-distal straight region of the 4HB (Fig. 1*D*). Based on the stalk domain adopting a 4HB structure, the possibility of successfully generating covalent dimers or tetramers is approximately equivalent. However, the model attributes preferential disulfide bond formation when residues at core positions are substituted for cysteine (shortest intersubunit Ca-Ca distances) (not shown).

Because bioactivity of the H-protein requires proper surface expression and receptor binding competence, we assessed intracellular transport competence and SLAM binding of the 25 single cysteine H mutants that were generated. While sur-

Motion within the Morbillivirus H-stalk Triggers Fusion

face expression levels of individual mutants varied somewhat, all H constructs but H-D101C were surface-expressed (supplemental Fig. S1). To determine receptor binding activity, we subjected H-protein mutants to a semi-quantitative SLAM binding assay that we have previously established (31). Clearly, all mutants exhibited proper interaction with SLAM, efficiency of binding fluctuated between 60 and 100% relative to Hwt (supplemental Fig. S1). With the exception of H-D101C, systematic cysteine mutagenesis of the central region of the H-stalk domain did thus not dramatically alter cell-surface expression and receptor binding activity of the molecule.

Unliganded CDV H-stalk Forms a Compact Tetramer—If the 4HB represents the conformation of the CDV H-stalk domain prior to receptor binding, cysteine substitutions at hydrophobic core positions should most efficiently engage in intermolecular disulfide bonds. Moreover, as inferred from the 4HB-stalk structural model, a successful covalent crosslink might either reinforce the covalently linked dimers or generate covalently linked tetramers. To test this, H-protein mutants were expressed in receptor-negative Vero cells, followed by harvesting of cell surface material through surface immunoprecipitation 1 day post-transfection. To efficiently resolve the high molecular weight H-dimers and tetramers, precipitated denatured material was fractionated on Tris/acetate gels under nonreducing conditions. In this system, Hwt migrated essentially as one single band, which corresponded to the molecular mass of the expected covalently linked dimers (~170 kDa) (14, 30) (Fig. 2A). In striking contrast, ~50% of the cysteine-stalk mutants examined generated an additional higher molecular weight H-antigenic population of ~340 kDa, corresponding to the expected mass of an H-tetramer (Fig. 2A). This observation therefore provided first evidence for successful engineering of covalently linked H-tetramers. Interestingly, the ratio of dimers *versus* tetramers did fluctuate among all mutants. Fig. 2A shows a representative gel for selected H-mutants, which followed three main phenotypes: 1) mutants H-V91C, G100C, G104C, L105C, and K115C migrated mostly as homo-dimers, 2) mutants H-I98C, R106C, L107C, and I114C exhibited an approximately equal distribution between dimers and tetramers, and 3) H-Q109C was predominantly found as covalently linked tetramer. It is generally assumed that reactive free thiols are prime targets for ER isomerases, resulting in intracellular retention and ultimately protein degradation (45). This is most likely the reason for the cell surface expression deficiencies that we observed for some of the H mutants.

To further assess whether selected H cysteine mutants generated intermolecular disulfide bonds, cysteine substitutions were introduced into two additional H variants. First, residues at position 98, 107, or 109 were changed to cysteine in an H-C139A/C154A background that lacks natural intermolecular disulfide bonds. Plasma membrane-exposed H material was isolated by surface immunoprecipitation and subjected to Western blot analysis using Tris/glycine gels. Under nonreducing conditions, both cell surface expression and dimerization capacities of H-C139A/C154A were strongly impaired as compared with Hwt (Fig. 2B). Importantly, both functions were efficiently restored in the case of triple mutants H-C139A/C154A/I98C and H-C139A/C154A/I107C and partially in the case of

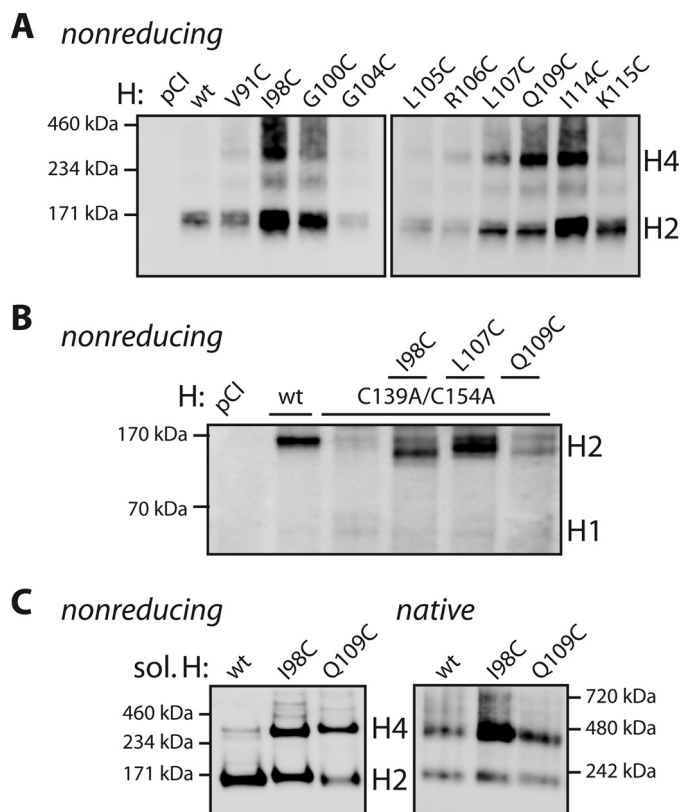


FIGURE 2. Successful engineering of intermonomers disulfide bonds. A, assessment of covalent H-tetramers. Surface-exposed material (surface immunoprecipitation; anti-FLAG mAb) of Vero cells transfected with plasmids encoding the various FLAG-tagged H-constructs, or empty plasmids (pCI) were analyzed. Precipitates were boiled and fractionated in Tris/acetate gels under nonreducing conditions, H-antigenic material was detected with a polyclonal anti-H antibody (41). H4: H-tetramers; H2: H-dimers; H1: H-monomers. B, assessment of disulfide bond formation in an H-C139A/C154A cysteine-free background. Vero cells transfected with plasmids encoding selected H mutants were lysed with stringent RIPA buffer. Lysates were boiled and fractionated in Tris/glycine gels under reducing and nonreducing conditions. H4: H-tetramers; H2: H-dimers; H1: H-monomers. C, assessment of disulfide bond generation in soluble H. Supernatants of transfected 293T cells were harvested 3 days post-transfection. Soluble H-proteins were then purified using nickel-based magnetic beads and 1 μ g of protein was then fractionated either in Tris/acetate gels (left panel) or in native gels (right panel). H-antigenic material was detected with the polyclonal anti-H antibody. H4: H-tetramers; H2: H-dimers; H1: H-monomers.

H-C139A/C154A/Q109C (Fig. 2B). Second, substitutions I98C and Q109C were introduced into soluble forms of Hwt (sol. H) that lacks the transmembrane domains and cytosolic tails. These soluble forms additionally carry the stabilizing dimeric/tetrameric GCN4 motif fused to its N-terminal region (supplemental Fig. S2A). Soluble H is recognized by a panel of previously described anti-H monoclonal antibodies (42) and selectively binds to cells expressing SLAM (supplemental Fig. S2, B and C). Mutating SLAM residues 70–73 to alanine, a known contact region for H (9), abrogated binding of sol. H and hence validated the overall proper folding of the soluble variant (supplemental Fig. S2D). Under denaturing and nonreducing conditions, purified sol. H and derivative mutants exhibited dimers/tetramers ratios very similar to those obtained before when the membrane-bound equivalents were analyzed. However, a small amount of non-covalently linked, GCN4-stabilized soluble H-tetramers resisted complete denaturation (Fig. 2C, left panel). When fractionated under native conditions, sol. H

returned a ~50% dimer/tetramers ratio, while both soluble H mutants with additional cysteine substitutions exhibited a higher proportion of tetrameric material (Fig. 2C, right panel).

In summary, these data provide strong biochemical evidence for successful intermolecular disulfide bond formation and are best compatible with a 4HB conformational state of the CDV H-stalk central region. Importantly, successful engineering of covalent H-tetramers at successive position along the central stalk region implies some degree of intra- and inter-helix rotational flexibility, which is consistent with the previously reported successful insertion of *N*-glycans at consecutive positions (residues 110–112) into the MeV H-stalk (27).

Reversible Fusion Inhibition Mediated by Engineered H-stalk Disulfide Bonds—We next assessed whether structural flexibility within the putative 4HB of the H mutants correlates with membrane fusion triggering. Toward this goal, we co-expressed Hwt or H derivatives with F in receptor-positive Vero-cSLAM cells. To synchronize the initiation of membrane fusion, transfected cells were treated overnight with a specific fusion inhibitor, termed 3g (36, 37). One day post-transfection, cells were washed and exposed to a low concentration of a reducing agent (DTT), or left untreated. Of the 25 cysteine H-mutants analyzed, 18 lost their capacity to support membrane fusion (Fig. 3A and supplemental Fig. S3). Remarkably, DTT treatment partially restored fusion activity in three out of the 18 fusion-support deficient mutants: H-I98C, L105C, and L107C (Fig. 3, A and B). Furthermore, H mutants G100C, G104C, R106C, and Q109C, which retained partial F-triggering functionality, exhibited a clear enhancement of membrane fusion promotion after DTT treatment (Fig. 3A). For a panel of selected H mutants, these results were confirmed in a luciferase-based quantitative fusion assay (Fig. 3C). Using the quantitative assay, we noted that treating the cells with DTT reduced the extent of Hwt/F-mediated fusion, because Hwt and H-K115C (also characterized by an Hwt-like fusion-promotion phenotype) exhibited an ~2-fold reduction in reporter activity-triggering in the presence of the reducing agent (Fig. 3C). This observation further strengthens the fusion-enhancing effect of some of the H disulfide mutants under partially reducing conditions. Since our results did not reveal any obvious correlation between the reversible fusion-inhibition phenotype of H mutants and the position of the different cysteine substitutions within the putative 4HB structure (Fig. 3B), the results further support the view that the central region of the H-stalk must be structurally flexible.

Overall, seven cysteine H mutants, which map along the central stalk region (98–109), are strongly impaired in membrane fusion promotion. Most importantly, their F-triggering capacities can be partially restored (or boosted) through short exposure to mild reducing conditions. Thus, our functional approach not only validated our biochemical data for successful generation of intermolecular disulfide bonds but illuminated, for the first time, that the central region of the CDV H-stalk subunits must be structurally flexible for efficient F-protein triggering.

Flexibility of the Central H-stalk Section Is Universally Required for Morbillivirus F-triggering—Based on the high sequence conservation of the central stalk section of the mor-

billivirus H-proteins (Fig. 1B), we next explored whether structural flexibility in this subdomain constitutes a general requirement for fusion triggering by morbilliviruses. To broaden the spectrum of morbillivirus representatives tested, we first introduced the I98C substitution into attachment proteins of two additional CDV H strains, H-OP (derived from the vaccine Onderstepoort strain) and H-301F (derived from a fox-isolate during the 2010 outbreak in Switzerland (32)). Strikingly, both H mutants essentially exhibited the same phenotype as Hwt: membrane fusion-promotion was strongly inhibited by the 98C-dependent disulfide bond formation, but this inhibitory effect was partially reversed under mildly reducing conditions (Fig. 4A and supplemental Fig. S4). We then expanded the study to H proteins derived from two different MeV strains by introducing the I98C substitution into the H proteins derived from the attenuated Edmonston strain (MeV-H (edm)) and the wild-type WTFb strain (MeV-H (WTFb)). Again, the F-triggering activity of the H variants was blocked, but membrane fusion could be restored through DTT treatment (Fig. 4B). Because it is well known that all MeV strains efficiently bind to the SLAM receptor while only laboratory-adapted strains also interact efficiently with CD46, we investigated whether the requirement for stalk flexibility is linked to entry through SLAM by examining the extent of cell-to-cell fusion in Vero cells that display CD46 but lack SLAM. A reversible fusion inhibition phenotype was observed also in this experimental setting. As expected, only the MeV-edm-derived H proteins induced efficient CD46-mediated fusion (Fig. 4C). Taken together, these results strongly suggest that structural flexibility of the central section of the attachment protein stalk is a universal requirement for morbillivirus H-mediated fusion triggering, independent of a specific morbillivirus strain or the nature of the viral receptor.

The Central Section of the H-stalk Encompasses F-contacting Residues—Functional assays based on heterologous F/H-protein pairings revealed that the stalk region 111–118 in MeV H contributes to efficient short-range interaction with F (23). Since we found that flexibility of the central stalk section (residues 98–109) is required for fusion triggering, we next expanded our cysteine-scanning mutagenesis to examine whether the homologous CDV H-stalk domain 111–114 also encompasses putative F-contacting amino acids. The resulting CDV H mutants were subjected to H/F co-immunoprecipitation (co-IP) experiments as previously described (35). Compared with co-precipitation of F proteins by Hwt, the H-mutants L111C, E113C, and I114C all showed a substantial reduction in F binding (Fig. 5A). This phenotype correlated with strong inhibition of fusion-support as shown above (Fig. 3A). In contrast, physical interaction of H-N112C with F was unaffected (Fig. 5A), and this variant returned Hwt-like fusion promotion activity (Fig. 3A). When mapped in the structural stalk model, residues 111, 113, and 114 located toward the middle region of the putative straight 4HB conformation of the stalk (Fig. 5C). Interestingly, the side chains of residues 111 and 114 are predicted to be located within the core 4HB structure (in “a” and “d” positions of the 11-mer repeat, respectively), whereas residue 113 is mostly surface exposed, making a direct contribution to physical contact with F conceivable (Fig. 5B). Alternatively, the actual configuration of the H-stalk may

Motion within the Morbillivirus H-stalk Triggers Fusion

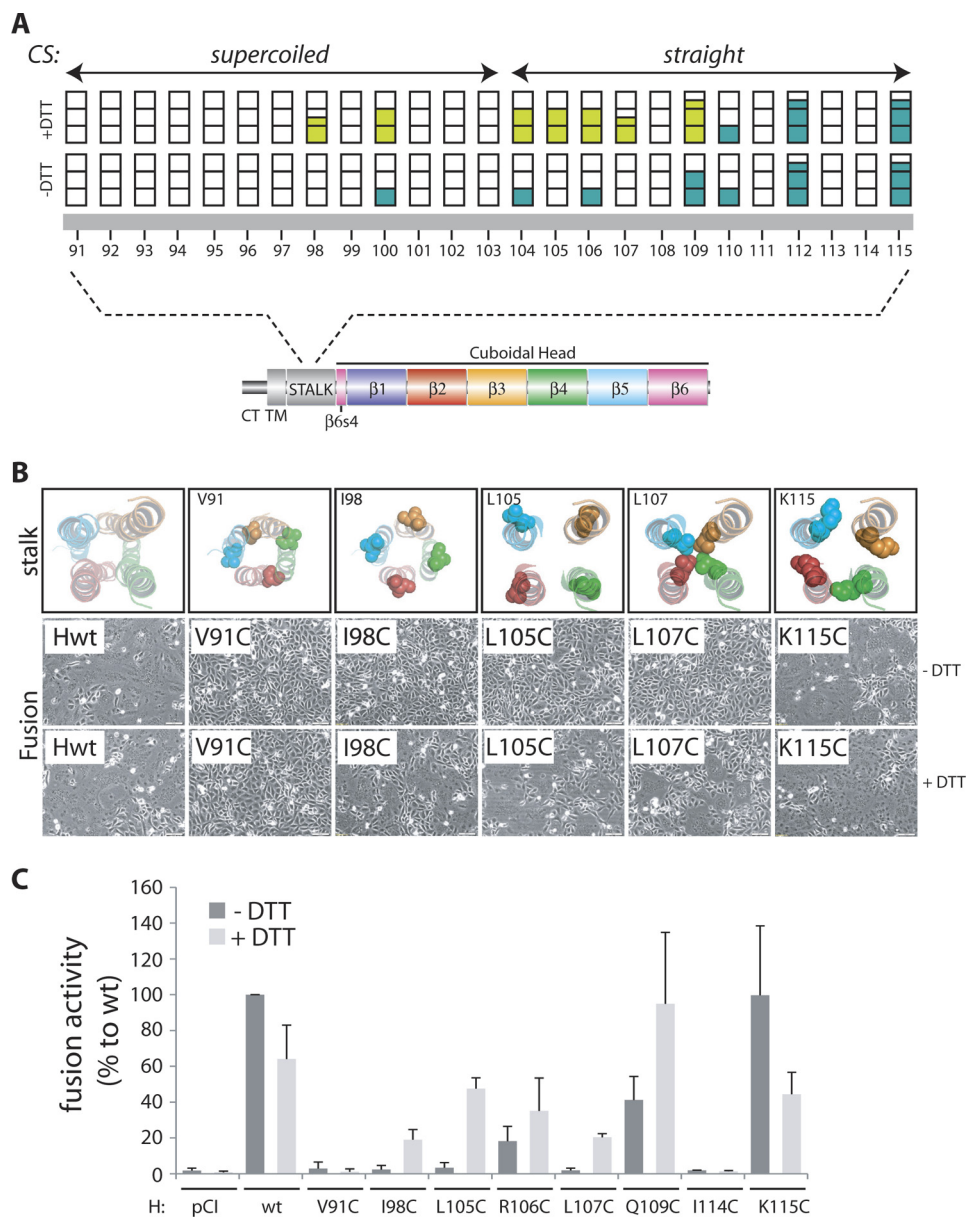


FIGURE 3. Reversible inhibition of F/H-induced cell-to-cell fusion by mild DTT-treatment. *A, upper panel:* graphic representation of fusion assay results, obtained in receptor-positive cells (Vero-cSLAM). Each bar represents a single cysteine substitution in the H-stalk sequence (*lower panel*; representation of H as in Fig. 1B). For fusion assays, Vero-cSLAM cells were transfected with plasmids encoding the F and H genes, followed by treatment overnight with a fusion-inhibiting molecule (36, 37). Fusion activity was analyzed 24 h post-transfection, after DTT treatment (30 min, 15 mM; +DTT), or without further treatment (-DTT). Each bar is partitioned in 3 parts, corresponding to three different levels of fusion-promotion activity of the different H mutants (0: no syncytium formation in 5 representative fields of views; 1: limited number of syncytia monitored in 5 representative fields of views; 2: intermediate numbers of syncytia monitored in 5 representative fields of views; 3: massive numbers of syncytia monitored in 5 representative fields of views). An average fusion score was assigned to each mutant based on three independent experiments. Bars filled with *dark green*: fusion activity promoted by the different H mutants; bars filled with *light green*, restored (or boosted) fusion activity after DTT-treatment. CS, crystal structure. *B, upper panels:* CDV H 4HB-stalk model; predicted positions of H-residue side chains of constructs that were selected for the quantitative fusion assays. Each monomer is color-coded. *Lower panels:* syncytium formation after co-transfection of Vero-cSLAM cells with plasmid DNA encoding various CDV-H proteins and F. Twenty-four hours post-transfection, cells were treated with DTT (15 mM) or left untreated; representative fields of view are shown. *C, quantitation of F-triggering activity of selected H mutants using a luciferase reporter gene-based content mix assay.* Vero-SLAM cells were infected with MVA-T7 (MOI of 1). In parallel, a second population (Vero cells) was transfected with plasmids encoding the different H proteins, a plasmid encoding F and a plasmid containing the luciferase reporter gene under the control of the T7 promoter. Twenty-four hours post-transfection, Vero cells were mixed with Vero-cSLAM cells and seeded into fresh plates. Cells were then incubated for 2 h in the presence of the fusion-inhibition molecule (3g), followed by extensive washing and incubation with or without DTT (15 mM) for 30 min. After 3 h at 37 °C, fusion was quantified using a commercial luciferase-measuring kit. For each experiment, luciferase activity of the F^{wt}/H^{wt} combination was set to 100%. Means and standard deviations of three independent experiments, performed in duplicate, are shown. *Dark gray histograms:* F/H-mediated fusion in the absence of DTT treatment; *Light gray histograms:* F/H-mediated fusion in the presence of DTT treatment.

somewhat differ from the homology model. This could affect the spatial organization of residues 111, 113, and 114, bringing them in direct contact with F. We finally tested the ability of the four H cysteine mutants to form covalent tetramers. Results

shown in Fig. 5D indicate efficient formation of intermolecular disulfide bond between the engineered cysteines. Fusion-promotion activity of those H mutants could not be restored (or enhanced) upon DTT treatment (Fig. 3A), suggesting that these

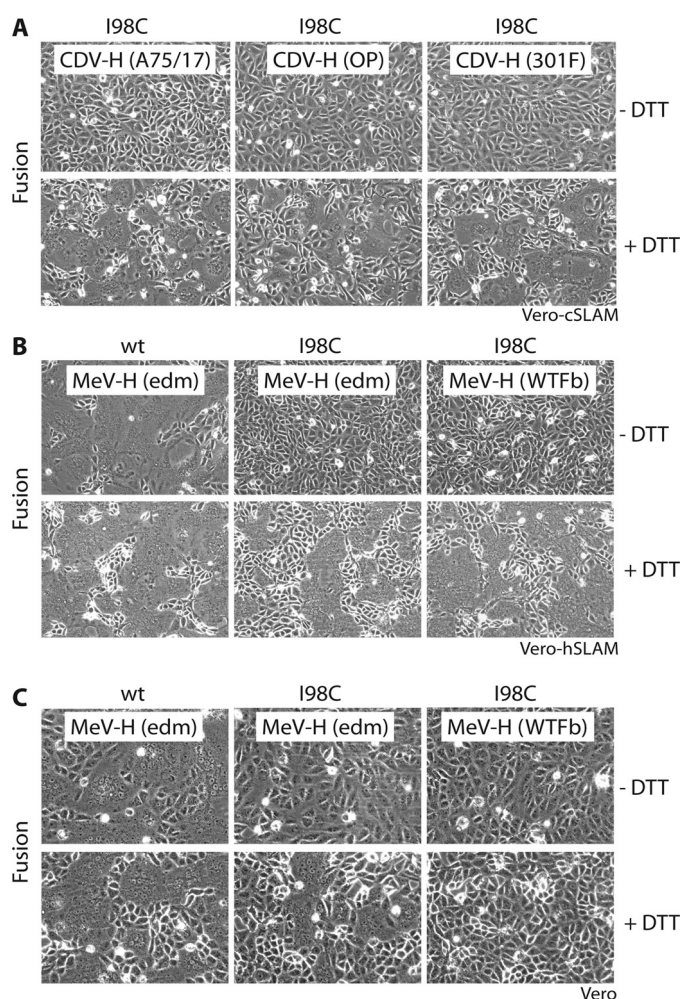


FIGURE 4. Structural flexibility of the central morbillivirus H-stalk region is universally required to trigger fusion. Syncytium formation after co-transfection of cells with plasmid DNA encoding various morbillivirus H and F proteins. After transfection, the cells were treated overnight with a fusion-inhibition molecule (3g for CDV and FIP for MeV). Twenty-four hours post-transfection, cells were washed and subsequently treated with DTT (15 mM) or left untreated; representative fields of view are shown. *A*, transfections were performed with CDV F and H-expression plasmids in Vero-cSLAM cells. *B*, transfections were performed with MeV F and H-expression plasmids in Vero-hSLAM cells. *C*, transfections were performed with MeV F and H-expression plasmids in Vero cells.

three substitutions distort the F contact site even when reduced to the free thiol, and thus never regain the ability to interact with F. In summary, these findings are consistent with the view that receptor binding triggers structural rearrangements of the H-stalk region 98–109, which in turn may affect the segment 111–114 that contributes to physical contact of H with F.

DISCUSSION

To achieve cell entry for viral dissemination, paramyxoviruses fuse their lipid envelope with host cell membranes at neutral pH. Although many studies implicated the stalk domain of the paramyxovirus attachment protein in transmitting fusion support to F (17, 18, 21, 23, 46), the molecular mechanism that links attachment protein receptor binding to triggering of the F protein for membrane fusion remains unresolved. In the present study, we employed a disulfide bond engineering strategy to probe molecular determinants for F-triggering by the morbilli-

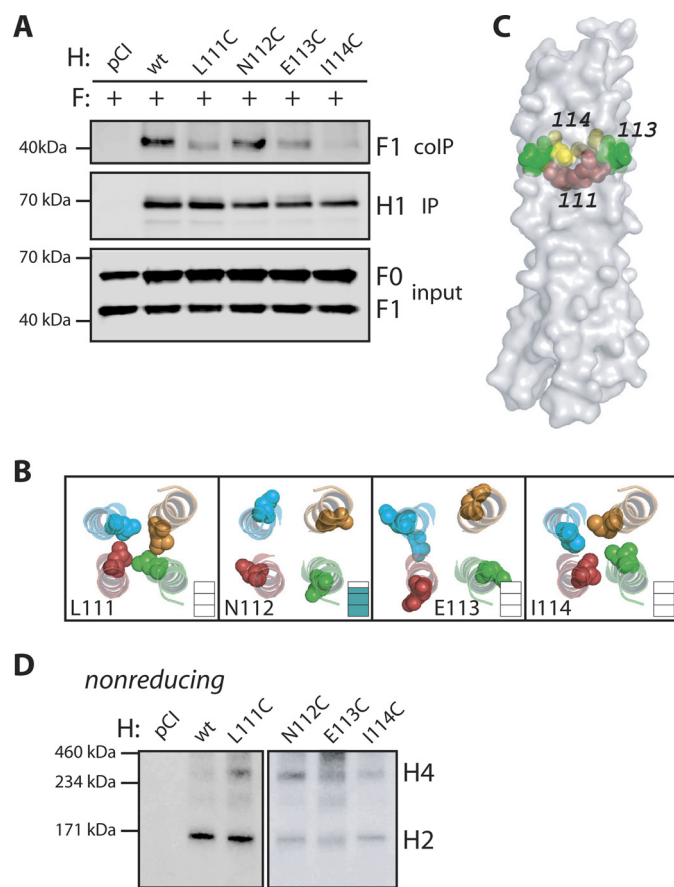


FIGURE 5. The 111–114 section of the CDV H-stalk domain regulates F binding activity. *A*, assessment of H interaction with functional F proteins. To stabilize the F/H interactions, Vero cells co-transfected with F- and H-expression plasmids (or empty plasmid: pCI) were treated with the membrane-impermeable crosslinker DTSSP. Subsequently, Vero cells were lysed with stringent RIPA buffer, followed by H immunoprecipitation (IP) with an anti-H mAb (1347) recognizing a linear epitope and protein G-Sepharose beads. Precipitates were boiled and subjected to immunoblotting using a polyclonal anti-F antiserum for F detection (41). In addition, F-proteins present in the lysates prior to IP were detected by immunoblot using a polyclonal anti-F antibody (TL). As a control, total H immunoprecipitates, were analyzed by immunoblotting using a polyclonal anti-H antibody (IP). *H1*: H-monomers; *F0*: uncleaved F precursors; *F1*: cleaved F precursors. *B*, CDV H 4HB-stalk model; the side chains of residues H-L111, H-N112, H-E113, and H-I114 are highlighted, and each residue is color-coded. *Inset*: fusion-triggering capacity of each H mutant (supplemental Fig. S3). *C*, surface representation of the structural model of the CDV H-stalk (bottom is membrane-proximal). Positions of residues H-L111 (in red), H-E113 (in green), and H-I114 (in yellow) are shown. *D*, assessment of covalent tetramerization of H variants harboring cysteine residues at consecutive positions from residue 111 to 114. Cell surface-exposed material was analyzed as detailed in Fig. 2A.

virus attachment protein. Our data illustrate that intersubunit rearrangements within the central region of the H-stalk are required for F activation, leading to a new model for Morbillivirus infection.

Successful engineering of supranumerical *N*-glycans into the central region of the MeV H-stalk at three consecutive positions has indicated high rotational flexibility of the individual stalk monomers relative to each other in this section (27). To restrict the degree of freedom for conformational rearrangements between the monomers in this region, we sought to add additional disulfide bonds to the stalk center through insertion of cysteine substitutions. The appearance of covalently linked H-tetramers confirmed in several cases that inter-dimeric

Motion within the Morbillivirus H-stalk Triggers Fusion

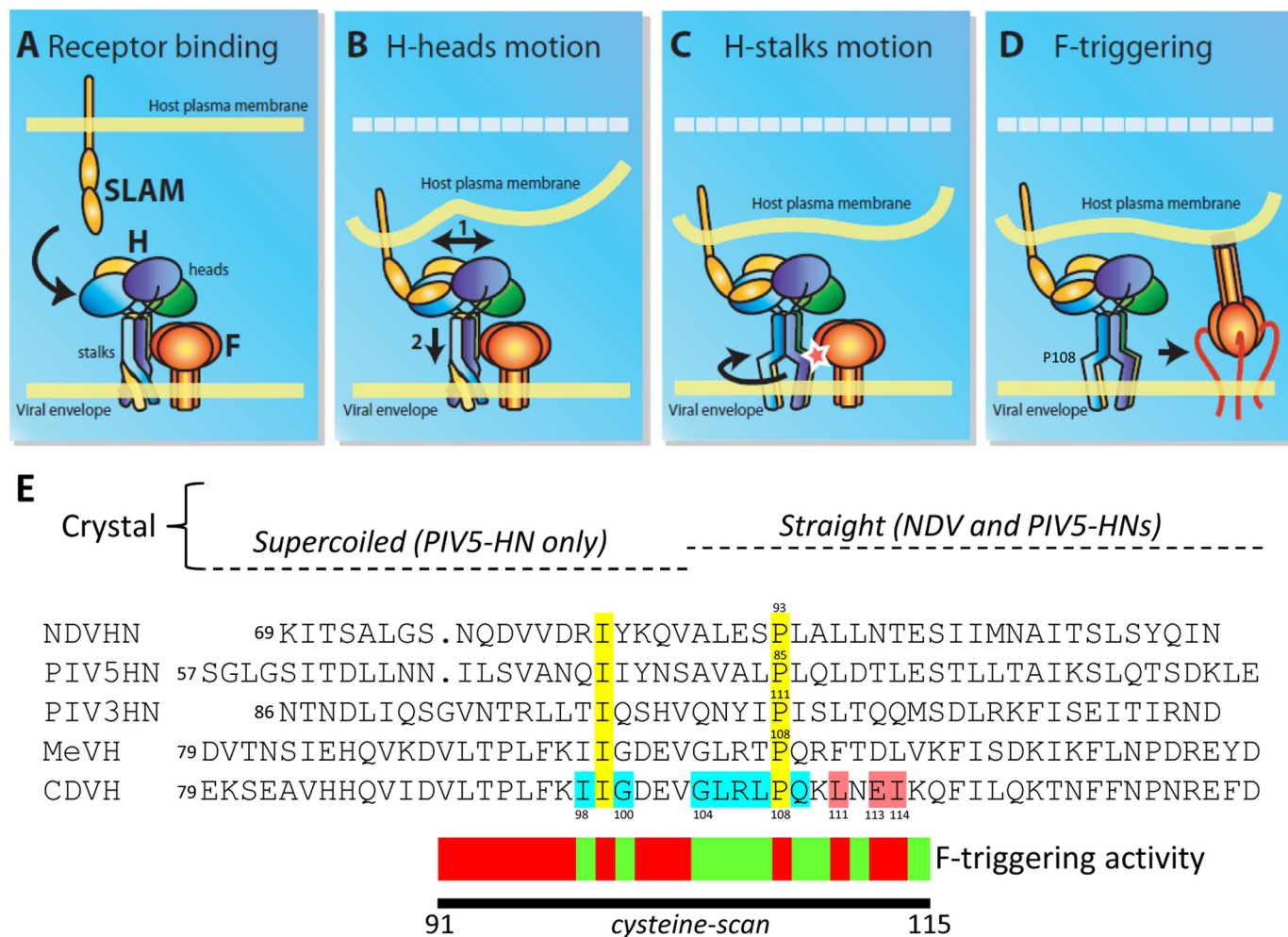


FIGURE 6. Model of paramyxovirus attachment protein-mediated F-triggering activity. *A*, prior to receptor binding, the tightly packed tetrameric attachment protein stalk domain, which supports the four receptor-binding heads, sustains physical interaction with F. *B*, upon receptor binding, the heads rearrange, in turn applying forces to the stalk and the transmembrane domains. Because SLAM is thought to bind to the H-head laterally (9), this may result in reducing the distance between target and effector membranes (initial position of the target membrane is represented by a dashed white line). *C*, putative metastable supercoiled lower section of the stalk then unwinds, thereby inducing intersubunits rearrangements of the central stalk region, which is predicted to contact F. This central section, and possibly the conserved proline residue at position 108, is then pivotal in F-triggering. The red star indicates active H-mediated F-triggering. *D*, activated F undergoes structural rearrangements, reaching the pre-hairpin state. *E*, upper section: sequence alignment of a partial section of the attachment protein stalk domains of several paramyxoviruses (NDV, PIV3 and 5, MeV and CDV). Yellow: conserved residues; light blue: residues identified in CDV H that are DTT-sensitive when mutated to cysteine (fusion activity restored or boosted). Light red: residues in CDV and MeV H (23) identified as contributors to F interaction. Lower section: representation of the segment targeted by cysteine-scanning mutagenesis. Individual mutants and the corresponding F-triggering capacities are shown above: light green color indicates DTT-dependent and/or independent fusion promotion; dark red color indicates strong deficiency in fusion promotion (both in the absence and presence of DTT treatment).

disulfide bonds were successfully introduced. Additionally, we obtained several lines of evidence that engineered disulfide bonds also formed between monomers of preexisting covalent H-dimers, restricting the rotational flexibility of the central sections of these stalk monomers relative to each other: (i) the model of the 4HB stalk conformation predicts every stalk monomer at equidistance from its neighbors, (ii) none of the constructs abolished intracellular transport competence of covalent H-dimers. We specifically investigated cell surface-exposed complexes, while H cysteine mutants with reactive free thiols are typically intracellularly retained and hence excluded (45), and (iii) membrane fusion inhibition was not strictly linked to covalent tetramer formation. For example, mutant H-Q109C, a potent inducer of covalent tetramers, very efficiently triggers F, while H-L105C, exhibiting almost no covalent H-tetramers, is incapable of initiating membrane fusion.

Crystallization of the NDV and PIV5 HN-stalk regions revealed a common membrane-distal straight 4HB that contains an 11-residue repeat encompassing putative F-binding residues (15, 16). Interestingly, the membrane-proximal region of the PIV5 HN-stalk structure features a supercoiled state, which exhibits a 7-residue repeat (15). Our disulfide engineering-based data are consistent with a close spatial proximity of all four H-stalk monomers prior to receptor-binding, which is best represented by a 4HB conformation. Alignment of the PIV5 HN-stalk sequence with MeV and CDV H posits residues 103 and 104 of Morbillivirus H at the junction between the supercoiled and the straight 4HB sections of the stalk (Fig. 6E). Remarkably, cysteine-scanning revealed a functional-switch (inhibition/induction of fusion triggering) that exactly coincides with this PIV5-stalk structural boundary (Fig. 6E).

These observations set the stage for a refined general model of paramyxovirinae attachment protein-mediated membrane fusion activity. We hypothesize that the supercoiled conformation of the lower part of the 4HB exists in a metastable state that may be transiently stabilized by the four membrane-anchored stalk domains. Prior to receptor binding, the central region of the tightly packed tetrameric attachment protein stalk sustains physical interaction with F (Fig. 6A). Upon receptor binding, the heads rearrange, in turn applying forces to the stalk and transmembrane domains (Fig. 6B). The postulated supercoiled lower section of the stalk then partially unwinds, which affect the adjacent stalk section contacting prefusion F (Fig. 6C). The resulting rearrangement of this central section may thus play a direct role in F-triggering (Fig. 6, C and D).

Consistent with this model, engineered intermolecular disulfide bonds in the lower stalk segment (91–97, 99, 101–103) completely abrogated F-triggering, probably by disturbing the metastable supercoiled structure and/or preventing supercoil unwinding, in essence destroying the driving force required for inducing rearrangements in the upper part of the stalk. Only cysteine substitution at positions 98 and 100 appeared to be tolerated within the metastable supercoiled state.

Cysteines inserted along the first straight 4HB segment (104–109) caused reversible fusion inhibition. This section may therefore not exist in a metastable state, but require rotational flexibility to trigger membrane fusion. Substitutions conducted within the more distal stalk segment encompassing positions 111, 113, and 114 severely impeded membrane fusion and could not be reactivated. This is consistent with coIP experiments previously reported (23) and described here, since these mutants are characterized by impaired physical interaction with F. In contrast, cysteine substitutions at positions 112 and 115 did not result in significant impairments in fusion-promotion, supporting the view that residues at these positions are not involved in essential F-binding and/or triggering activities. Taken together, we propose that structural rearrangements between H-stalk monomers are universally required for F-protein triggering. This is based on the remarkable amino acid sequence conservation of the central stalk region (90–109) across different H-proteins and our finding that H-mutant I98C consistently returns a reversible fusion-inhibition phenotype in the panel of CDV and MeV strains investigated.

Within the realms of the proposed model, structural rearrangements involving the central section of the H-stalk represent a terminal state leading to F-triggering. Early signals may be generated by receptor binding of the H-heads, initiating changes within the spatial organization of the oligomeric head domains. In the case of MeV H, Hashiguchi *et al.* (9) suggested that the covalently linked H-head dimers move as blocks relative to each other, a structural motion that might be preceded by minor adjustments within the heads' dimer interface (30). While the atomic structure of the PIV5 HN-tetramer exhibited a largely planar configuration (47), the recently reported crystal structure of the NDV HN-protein revealed a yet unanticipated tetrameric conformation (16). In the latter structure, both HN-head dimers are not engaged in direct physical interactions, but the lower head of each dimer contacts the 4HB stalk domain. Because the connectors linking the upper 4HB stalk to the

heads were not revealed in the available x-ray structures, spatial flexibility of this domain was inferred. It is conceivable that the NDV HN-heads may rearrange upon receptor-binding, in turn affecting the 4HB stalk conformation as recently proposed by Yuan *et al.* (16) for NDV HN-mediated F-triggering. As both models implicate structural modifications of the membrane-proximal stalk domain in F-triggering, our disulfide engineering-based findings may apply to paramyxovirinae glycoprotein-mediated membrane fusion in general beyond the morbillivirus system.

Acknowledgments—We thank Laurent Roux, Jürgen Schneider-Schaulies, and Veronika von Messling for providing the pTM-Luc plasmid, MeV F and H expression plasmids and the Vero cSLAM cells, respectively. We also thank Giuseppe Bertoni for helpful comments on the manuscript.

REFERENCES

- Chen, S. Y., Anderson, S., Kutty, P. K., Lugo, F., McDonald, M., Rota, P. A., Ortega-Sanchez, I. R., Komatsu, K., Armstrong, G. L., Sunenshine, R., and Seward, J. F. (2011) Health care-associated measles outbreak in the United States after an importation: challenges and economic impact. *J. Infect. Dis.* **203**, 1517–1525
- Tatsuo, H., Ono, N., Tanaka, K., and Yanagi, Y. (2000) SLAM (CDw150) is a cellular receptor for measles virus. *Nature* **406**, 893–897
- Tatsuo, H., Ono, N., and Yanagi, Y. (2001) Morbilliviruses use signaling lymphocyte activation molecules (CD150) as cellular receptors. *J. Virol.* **75**, 5842–5850
- Dörig, R. E., Marcil, A., Chopra, A., and Richardson, C. D. (1993) The human CD46 molecule is a receptor for measles virus (Edmonston strain). *Cell* **75**, 295–305
- Negrete, O. A., Levroney, E. L., Aguilar, H. C., Bertolotti-Ciarlet, A., Nazarian, R., Tajyar, S., and Lee, B. (2005) EphrinB2 is the entry receptor for Nipah virus, an emergent deadly paramyxovirus. *Nature* **436**, 401–405
- Bonaparte, M. I., Dimitrov, A. S., Bossart, K. N., Crameri, G., Mungall, B. A., Bishop, K. A., Choudhry, V., Dimitrov, D. S., Wang, L. F., Eaton, B. T., and Broder, C. C. (2005) Ephrin-B2 ligand is a functional receptor for Hendra virus and Nipah virus. *Proc. Natl. Acad. Sci. U.S.A.* **102**, 10652–10657
- Negrete, O. A., Wolf, M. C., Aguilar, H. C., Enterlein, S., Wang, W., Mühlberger, E., Su, S. V., Bertolotti-Ciarlet, A., Flick, R., and Lee, B. (2006) Two key residues in ephrinB3 are critical for its use as an alternative receptor for Nipah virus. *PLoS Pathog.* **2**, e7
- Lamb, R. A., and Parks, G. D. (2007) In *Paramyxoviridae: The Viruses and their Replication*, Fields Virology (Knipe, D. M. and Howley, P. M., eds) 5 Ed., Wolters Kluwer/Lippincott Williams & Wilkins, Philadelphia
- Hashiguchi, T., Ose, T., Kubota, M., Maita, N., Kamishikiryō, J., Maenaka, K., and Yanagi, Y. (2011) Structure of the measles virus hemagglutinin bound to its cellular receptor SLAM. *Nat. Struct. Mol. Biol.* **18**, 135–141
- Santiago, C., Celma, M. L., Stehle, T., and Casasnovas, J. M. (2010) Structure of the measles virus hemagglutinin bound to the CD46 receptor. *Nat. Struct. Mol. Biol.* **17**, 124–129
- Hashiguchi, T., Kajikawa, M., Maita, N., Takeda, M., Kuroki, K., Sasaki, K., Kohda, D., Yanagi, Y., and Maenaka, K. (2007) Crystal structure of measles virus hemagglutinin provides insight into effective vaccines. *Proc. Natl. Acad. Sci. U.S.A.* **104**, 19535–19540
- Colf, L. A., Juo, Z. S., and Garcia, K. C. (2007) Structure of the measles virus hemagglutinin. *Nat. Struct. Mol. Biol.* **14**, 1227–1228
- Brindley, M. A., and Plemper, R. K. (2010) Blue native PAGE and biomolecular complementation reveal a tetrameric or higher-order oligomer organization of the physiological measles virus attachment protein H. *J. Virol.* **84**, 12174–12184
- Plemper, R. K., Hammond, A. L., and Cattaneo, R. (2000) Characterization of a region of the measles virus hemagglutinin sufficient for its dimeriza-

Motion within the Morbillivirus H-stalk Triggers Fusion

- tion. *J. Virol.* **74**, 6485–6493
15. Bose, S., Welch, B. D., Kors, C. A., Yuan, P., Jardetzky, T. S., and Lamb, R. A. (2011) Structure and mutagenesis of the parainfluenza virus 5 hemagglutinin-neuraminidase stalk domain reveals a four-helix bundle and the role of the stalk in fusion promotion. *J. Virol.* **85**, 12855–12866
 16. Yuan, P., Swanson, K. A., Leser, G. P., Paterson, R. G., Lamb, R. A., and Jardetzky, T. S. (2011) Structure of the Newcastle disease virus hemagglutinin-neuraminidase (HN) ectodomain reveals a four-helix bundle stalk. *Proc. Natl. Acad. Sci. U.S.A.* **108**, 14920–14925
 17. Deng, R., Wang, Z., Mirza, A. M., and Iorio, R. M. (1995) Localization of a domain on the paramyxovirus attachment protein required for the promotion of cellular fusion by its homologous fusion protein spike. *Virology* **209**, 457–469
 18. Tsurudome, M., Kawano, M., Yuasa, T., Tabata, N., Nishio, M., Komada, H., and Ito, Y. (1995) Identification of regions on the hemagglutinin-neuraminidase protein of human parainfluenza virus type 2 important for promoting cell fusion. *Virology* **213**, 190–203
 19. Tanabayashi, K., and Compans, R. W. (1996) Functional interaction of paramyxovirus glycoproteins: identification of a domain in Sendai virus HN which promotes cell fusion. *J. Virol.* **70**, 6112–6118
 20. Deng, R., Mirza, A. M., Mahon, P. J., and Iorio, R. M. (1997) Functional chimeric HN glycoproteins derived from Newcastle disease virus and human parainfluenza virus-3. *Arch. Virol. Suppl* **13**, 115–130
 21. Wang, Z., Mirza, A. M., Li, J., Mahon, P. J., and Iorio, R. M. (2004) An oligosaccharide at the C-terminus of the F-specific domain in the stalk of the human parainfluenza virus 3 hemagglutinin-neuraminidase modulates fusion. *Virus Res.* **99**, 177–185
 22. Plemper, R. K. (2011) Cell Entry of Enveloped Viruses. *Curr. Opin. Virol.* **1**, 92–100
 23. Lee, J. K., Prussia, A., Paal, T., White, L. K., Snyder, J. P., and Plemper, R. K. (2008) Functional interaction between paramyxovirus fusion and attachment proteins. *J. Biol. Chem.* **283**, 16561–16572
 24. Tsurudome, M., Ito, M., Nishio, M., Kawano, M., Okamoto, K., Kusagawa, S., Komada, H., and Ito, Y. (1998) Identification of regions on the fusion protein of human parainfluenza virus type 2, which are required for haemagglutinin-neuraminidase proteins to promote cell fusion. *J. Gen. Virol.* **79**, 279–289
 25. Tsurudome, M., Ito, M., Nishio, M., Nakahashi, M., Kawano, M., Komada, H., Nosaka, T., and Ito, Y. (2011) Identification of domains on the fusion (F) protein trimer that influence the hemagglutinin-neuraminidase specificity of the f protein in mediating cell-cell fusion. *J. Virol.* **85**, 3153–3161
 26. Wild, T. F., Fayolle, J., Beauverger, P., and Buckland, R. (1994) Measles virus fusion: role of the cysteine-rich region of the fusion glycoprotein. *J. Virol.* **68**, 7546–7548
 27. Paal, T., Brindley, M. A., St. Clair, C., Prussia, A., Gaus, D., Krumm, S. A., Snyder, J. P., and Plemper, R. K. (2009) Probing the spatial organization of measles virus fusion complexes. *J. Virol.* **83**, 10480–10493
 28. Aguilar, H. C., Ataman, Z. A., Aspericueta, V., Fang, A. Q., Stroud, M., Negrete, O. A., Kammerer, R. A., and Lee, B. (2009) A novel receptor-induced activation site in the Nipah virus attachment glycoprotein (G) involved in triggering the fusion glycoprotein (F). *J. Biol. Chem.* **284**, 1628–1635
 29. Bishop, K. A., Hickey, A. C., Khetawat, D., Patch, J. R., Bossart, K. N., Zhu, Z., Wang, L. F., Dimitrov, D. S., and Broder, C. C. (2008) Residues in the stalk domain of the hendra virus g glycoprotein modulate conformational changes associated with receptor binding. *J. Virol.* **82**, 11398–11409
 30. Navaratnarajah, C. K., Oezguen, N., Rupp, L., Kay, L., Leonard, V. H., Braun, W., and Cattaneo, R. (2011) The heads of the measles virus attachment protein move to transmit the fusion-triggering signal. *Nat. Struct. Mol. Biol.* **18**, 128–134
 31. Zipperle, L., Langedijk, J. P., Orvell, C., Vandeveld, M., Zurbriggen, A., and Plattet, P. (2010) Identification of key residues in virulent canine distemper virus hemagglutinin that control CD150/SLAM binding activity. *J. Virol.* **84**, 9618–9624
 32. Origgi, F. C., Plattet, P., Sattler, U., Robert, N., Casaubon, J., Mavrot, F., Pewsner, M., Wu, N., Giovannini, S., Oevermann, A., Stoffel, M. H., Gaschen, V., Segner, H., and Ryser-Degiorgis, M. P. (2012) Emergence of Canine Distemper Virus strains with modified signature and enhanced neuronal tropism to high mortality in wild carnivores. *Vet. Pathol.*, in press
 33. Harbury, P. B., Zhang, T., Kim, P. S., and Alber, T. (1993) A switch between two-, three-, and four-stranded coiled coils in GCN4 leucine zipper mutants. *Science* **262**, 1401–1407
 34. Yuchi, Z., Pau, V. P., and Yang, D. S. (2008) GCN4 enhances the stability of the pore domain of potassium channel KcsA. *FEBS J.* **275**, 6228–6236
 35. Langedijk, J. P., Janda, J., Origgi, F. C., Örvell, C., Vandeveld, M., Zurbriggen, A., and Plattet, P. (2011) Canine distemper virus infects canine keratinocytes and immune cells by using overlapping and distinct regions located on one side of the attachment protein. *J. Virol.* **85**, 11242–11254
 36. Sun, A., Prussia, A., Zhan, W., Murray, E. E., Doyle, J., Cheng, L. T., Yoon, J. J., Radchenko, E. V., Palyulin, V. A., Compans, R. W., Liotta, D. C., Plemper, R. K., and Snyder, J. P. (2006) Nonpeptide inhibitors of measles virus entry. *J. Med. Chem.* **49**, 5080–5092
 37. Singethan, K., Hiltensperger, G., Kendl, S., Wohlfahrt, J., Plattet, P., Holzgrabe, U., and Schneider-Schaulies, J. (2010) N-(3-Cyanophenyl)-2-phenylacetamide, an effective inhibitor of morbillivirus-induced membrane fusion with low cytotoxicity. *J. Gen. Virol.* **91**, 2762–2772
 38. Nussbaum, O., Broder, C. C., and Berger, E. A. (1994) Fusogenic mechanisms of enveloped-virus glycoproteins analyzed by a novel recombinant vaccinia virus-based assay quantitating cell fusion-dependent reporter gene activation. *J. Virol.* **68**, 5411–5422
 39. Plattet, P., Cherpillod, P., Wiener, D., Zipperle, L., Vandeveld, M., Wittek, R., and Zurbriggen, A. (2007) Signal peptide and helical bundle domains of virulent canine distemper virus fusion protein restrict fusogenicity. *J. Virol.* **81**, 11413–11425
 40. Sutter, G., Ohlmann, M., and Erfle, V. (1995) Non-replicating vaccinia vector efficiently expresses bacteriophage T7 RNA polymerase. *FEBS Lett.* **371**, 9–12
 41. Cherpillod, P., Beck, K., Zurbriggen, A., and Wittek, R. (1999) Sequence analysis and expression of the attachment and fusion proteins of canine distemper virus wild-type strain A75/17. *J. Virol.* **73**, 2263–2269
 42. Orvell, C., Sheshberadaran, H., and Norrby, E. (1985) Preparation and characterization of monoclonal antibodies directed against four structural components of canine distemper virus. *J. Gen. Virol.* **66**, 443–456
 43. Peitsch, M. C. (1996) ProMod and Swiss-Model: Internet-based tools for automated comparative protein modelling. *Biochem. Soc. Trans.* **24**, 274–279
 44. Guex, N., and Peitsch, M. C. (1997) SWISS-MODEL and the Swiss-PDB-Viewer: an environment for comparative protein modeling. *Electrophoresis* **18**, 2714–2723
 45. Feige, M. J., and Hendershot, L. M. (2011) Disulfide bonds in ER protein folding and homeostasis. *Curr. Opin. Cell Biol.* **23**, 167–175
 46. Deng, R., Wang, Z., Mahon, P. J., Marinello, M., Mirza, A., and Iorio, R. M. (1999) Mutations in the Newcastle disease virus hemagglutinin-neuraminidase protein that interfere with its ability to interact with the homologous F protein in the promotion of fusion. *Virology* **253**, 43–54
 47. Yuan, P., Thompson, T. B., Wurzburg, B. A., Paterson, R. G., Lamb, R. A., and Jardetzky, T. S. (2005) Structural studies of the parainfluenza virus 5 hemagglutinin-neuraminidase tetramer in complex with its receptor, sialyllactose. *Structure.* **13**, 803–815